Journal of Power Sources 195 (2010) 6671–6679

Contents lists available at ScienceDirect

Journal of Power Sources

journal homepage: www.elsevier.com/locate/jpowsour

A particle-based model for predicting the effective conductivities of composite electrodes

Jay Sanyal[a], Graham M. Goldin[a], Huayang Zhu[b], Robert J. Kee[b,*]

[a] Ansys Inc., Lebanon, NH 03766, USA
[b] Engineering Division, Colorado School of Mines, Golden, CO 80401, USA

ARTICLE INFO

Article history:
Received 25 February 2010
Received in revised form 5 April 2010
Accepted 6 April 2010
Available online 13 April 2010

Keywords:
SOFC
Composite electrode
Effective conductivity
Percolation theory

ABSTRACT

This paper develops particle-resolved simulations to predict conductivity within porous composite electrodes. Hundreds of spherical particles (order fractions of a micron) are packed randomly into a cubical region (order of a few microns), using two alternative packing algorithms. The composite structures include both ion-conducting and electron-conducting particles. The particle network is discretized using tetrahedral meshes that fully resolve the interiors of the particles and their intersections. Charge-conservation equations are solved to predict current through the network. These simulations are used to derive the effective conductivities that are required for macroscale simulations at length scales much larger than the particle scale. Because the microstructures are synthesized via random particle packing, multiple realizations are needed to deliver statistically invariant results. The results show that a few hundred particles with a few hundred realizations is sufficient. Predicted coordination numbers, percolation probabilities, and three-phase-boundary lengths are consistent with percolation theory, but the predicted effective conductivities are significantly smaller than those predicted with conventional percolation theory. By adjusting the Bruggeman factor from the conventional value of 1.5–3.5 brings the percolation-theory prediction for effective conductivity in line with the fully resolved results.

1. Introduction

The objective of this paper is to develop microstructural models of composite electrodes that assist in predicting effective properties that can be used in larger scale continuum models. An anode-supported tubular SOFC, such as illustrated in Fig. 1, might be on the order of 100 mm long and 10 mm in diameter. A typical cell uses a relatively thick Ni–YSZ composite anode (around 1 mm) with a thin YSZ dense electrolyte (around 10 μm) and a thin LSM–YSZ composite cathode (around 50 μm). It is well established that SOFC performance depends greatly upon the structure of the composite electrodes [1]. Thus, there is a need to develop predictive models that can assist optimizing the cell architecture. The present paper is concerned with models that describe solid-phase ion and electron transport at the particle scale (submicron) within composite electrodes. The particular objective is to predict effective conductivity of a particle matrix as a function of particle size and packing structure. Although the work is motivated primarily by solid-oxide fuel cells (SOFC), the approach and results are considerably more general.

Porous composite electrodes involve three phases. The ion-conducting phase (typically yttria-stabilized zirconia, YSZ, is used in both the anode and cathode) must be a good oxygen-ion O^{2-} conductor, with very little electronic conduction. The electron-conducting phase (typically nickel, Ni, in the anode and strontium-doped lanthanum manganate, LSM, in the cathode) must have good electronic conduction, with very little ionic conduction. The pore phase must facilitate gas transport. Typically each of these three phases occupies about one third of the overall volume. Charge-transfer reactions proceed at the three-phase boundaries that are formed at the intersections of the three phases. The solid-phase particles and the pore spaces are typically on the order of a fraction of a micron.

The composite electrode must accomplish several essential functions. The electron-conducting phase must provide a low-resistance path from the position where the electrons are produced (or consumed) to the current collection. That is to say the electronic-conducting phase must percolate through the thickness of the composite electrode. Especially within a few tens of microns around the dense electrolyte the ion-conducting phase must percolate, enabling ion-conduction to the three-phase boundaries [2]. When hydrocarbon fuels are used, the Ni phase in the anode also serves as a reforming catalyst.

A structure that facilitates one function can sometimes serve to frustrate another function. For example, small particles and pore

* Corresponding author. Tel.: +1 303 273 3379; fax: +1 303 273 3602.
E-mail address: rjkee@mines.edu (R.J. Kee).

0378-7753/$ – see front matter © 2010 Elsevier B.V. All rights reserved.
doi:10.1016/j.jpowsour.2010.04.013

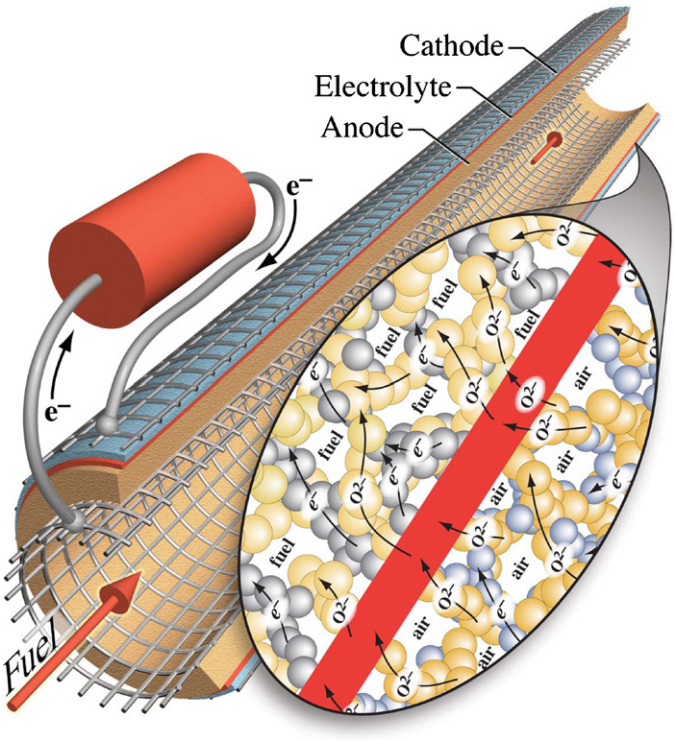

Fig. 1. Illustration of a tubular solid-oxide fuel cell. The balloon shows geometrical and functional aspects of the membrane-electrode assembly at the particle scale.

spaces tend to increase three-phase-boundary length, which facilitates the essential charge-transfer chemistry. However, the small pore spaces also serve to increase gas-transport resistance, which diminishes performance. Small particles can also decrease effective ionic and electronic conductivity, which can negatively influence performance. Because there are different functional needs in different regions of the composite electrode, functional grading of the electrode can improve performance. For example, in the few tens of microns near the dense electrolyte layer charge transfer is most important [2]. In this region a functional layer with fine particles and small pore spaces is valuable. However, far from the dense electrolyte there is no charge-transfer chemistry (i.e., all available charge has been transferred nearer to the dense electrolyte). In this region (usually the majority of an anode support structure) performance is improved by using large pores that minimize gas-transport resistance. Finding optimal electrode architectures that balance competing tradeoffs can be challenging and there is a need to understand quantitatively the influence of electrode structure on performance.

At the relatively large cell scale (e.g., the tube in Fig. 1) models cannot resolve details at the particle scale [3]. The approach in the present paper begins by synthesizing three-dimensional microstructures using packed, partially overlapping, spherical particles. From these random arrays of particles, geometrical characteristics such as coordination number, percolation probability, and three-phase-boundary length can be evaluated. With arrays of submicron particles in a three-dimensional domain of a few microns, it is possible model transport through the fully resolved complex particle network. From the solutions of such microscale models, it is possible to extract the effective conductivities that are needed to model transport at the macroscale. The paper compares effective properties derived from the fully resolved models with those derived from percolation theory.

2. Prior literature

A significant and growing body of literature is devoted to understanding complex electrode structure and performance at the microscale. Experimental investigations include measuring three-dimensional microstructure using a range of reconstruction techniques. In some cases the measurements are correlated to electrochemical performance. Other investigators use analytical and computation methods to synthesize and model microstructures.

Some investigators measure the structure of actual electrodes. Beginning with Wilson et al. [4], several groups have developed focused-ion-beam–scanning-electron-microscope (FIB–SEM) experiments to reconstruct composite electrodes [5–12]. Izzo et al. have developed similar electrode reconstructions of actual electrodes using X-ray tomography [13,14]. These investigations provide a great deal of quantitative information about the complexity of actual electrodes. Stereological imaging and reconstruction provide high-resolution measurements of three-phase-boundary (TPB) lengths, phase volumes, specific surface and interface areas, phase connectivity (percolation), and tortuosity. Such measurements can be used to validate the simulated electrode microstructures.

Monte-Carlo stochastic simulation techniques have been used to represent electrode microstructures. Electron- and ion-conducting particles can be either randomly packed [15–18] or randomly distributed on lattice structures [19]. Random particle networks can be further modified by numerical-sintering algorithms to represent the composite electrodes more accurately. Electrode structures can also be generated by using stochastic reconstruction schemes, which are based upon spatial statistical correlations that are derived from experimental images [20,21].

Reconstructed microstructures, either measured experimentally or synthesized computationally, can be used in models to investigate the interactions of microstructure with the operating performance [11]. Electrode reconstructions can also be parameterized for incorporation into macroscopic-scale models, thus effectively bridging scales from microstructure to cell performance [10,22]. Important microstructural parameters include TPB length, phase volume, phase surface and interface areas, phase connectivity and conductivity, and phase tortuosity.

Several investigations have been concerned with evaluating phase tortuosity. Gostovic et al. [5] and Smith et al. [10] calculated tortuosity by tracking the pore-center locations and evaluating effective path lengths. Wilson et al. [4] evaluated the tortuosity by converting the measured three-dimensional phase structures into finite-element meshes and solving steady-state diffusion equations. An alternative approach is to apply a lattice Boltzmann method (LBM) to solve a diffusion equation and derive a measure of phase tortuosity [23,20,13,24,12]. Iwai et al. [12] showed that a random-walk method and the LBM approach produced similar measures of tortuosity.

Grid-based counting techniques have been widely used to estimate TPB length [25,20,6,8,7,26]. Iwai et al. [12] developed a volume-expansion method and a centroid method to estimate the TPB length. Percolation theory and coordination number are also used to evaluate the active TPB length in synthesized microstructures [15–18].

Although experimental reconstructions provide specific details of complex microstructures, they offer relatively little predictive capability. Simulation techniques, although not representing actual microstructures exactly, provide a valuable tool for predicting the performance of alternative electrode architectures. By using measurements to validate microstructural-synthesis techniques, the predictive ability of simulation-based analysis is improved.

3. Percolation theory

At the macroscale, ion and electron transport is usually represented using the charge-conservation equations as

$$\nabla \cdot (\sigma_m^{\mathrm{e}} \nabla \Phi_m) + R_m = 0, \tag{1}$$

where σ_m^{e} (m = ed for the electronic-conducting phase, and m = el for the ionic-conducting phase) are the effective conductivities, Φ_m are the electric potentials, and R_m are the net charge-transfer rates. The challenge is to determine the effective conductivity in the way that represents the complexities of the porous composite electrodes. Effective conductivities can be approximated based upon coordination-number theory and the percolation theory as [27],

$$\sigma_m^{\mathrm{e}} = \sigma_m^0 [(1-\phi_{\mathrm{g}})\psi_m P_m]^{\gamma}, \tag{2}$$

where σ_m^0 are the conductivities of the bulk material (i.e., material from which particles are formed), ϕ_{g} is the porosity, ψ_m are the volume fractions based on solids alone (e.g., $\psi_{\mathrm{Ni}} = 0.5$ and $\psi_{\mathrm{YSZ}} = 0.5$ means that a composite Ni–YSZ anode is composed of 50% Ni and 50% YSZ), and γ is called the Bruggeman factor that accounts for tortuous conduction pathways. The Bruggeman factor is typically assumed to be $\gamma = 1.5$. The probability of percolation P_m represents the probability that the m-phase particles form a connected pathway through the electrode, enabling continuous conduction.

Bouvard and Lange [28] evaluated the probability of an m-phase particle being in a percolated cluster of the same phase as

$$P_m = \left[1 - \left(\frac{4 - Z_{mm}}{2}\right)^{2.5}\right]^{0.4}, \tag{3}$$

where the coordination number Z_{mm} is the average number of the m-phase particle neighbors of an m-phase particle. Assuming all the particles have the same size, Z_{mm} can be expressed as $Z_{mm} = \psi_m \bar{Z}$ where $\bar{Z}$ is the overall average coordination number, which is the average number of contacts that a particular particle makes with neighboring particles, independent of the phase or material identity of the particles. It is often assumed that $\bar{Z} = 6$ in a random packing of binary spheres.

Kuo and Gupta [29] showed that the percolation threshold is $Z_{mm}^{\mathrm{c}} = 1.764$, below which no cluster connecting both ends of the electrode is possible. Suzuki and Oshima [30] proposed a more accurate expression for the percolation probability as,

$$P_m = \left[1 - \left(\frac{4.236 - Z_{mm}}{2.742}\right)^{2.5}\right]^{0.4}, \tag{4}$$

which has zero probability at the percolation threshold.

The percolated three-phase-boundary (TPB) length per unit volume can also be predicted from the percolation theory as [31]

$$\lambda_{\mathrm{TPB}}^{\mathrm{V}} = \ell_{\text{ed-el}} n_{\mathrm{ed}} Z_{\text{ed-el}} P_{\mathrm{ed}} P_{\mathrm{el}}, \tag{5}$$

where $\ell_{\text{ed-el}} = 2\pi r \sin\theta$ is the contact perimeter between an ion-conducting particle and an electron-conducting particle. As illustrated in Fig. 2, the particle radius is r and the contact angle is θ. $Z_{\text{ed-el}}$ is the average coordination number between ion- and electron-conducting particles, and $Z_{\text{ed-el}} = \psi_{\mathrm{el}} \bar{Z}$ when the particles have the same size. P_{ed} and P_{el} are the percolation probabilities of electron- and ion-conducting particles, respectively. The number of the electron-conducting particles per unit volume within the entire composite electrode n_{ed} can be evaluated as $n_{\mathrm{ed}} = n_{\mathrm{tot}} \psi_{\mathrm{ed}}$ where n_{tot} is the total number of particles per unit volume,

$$n_{\mathrm{tot}} = \frac{1 - \phi_{\mathrm{g}}}{(4/3)\pi r^3}. \tag{6}$$

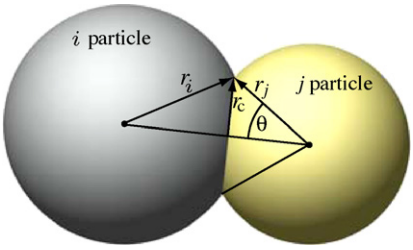

Fig. 2. Illustration of particle overlap angle. For different sized particles, the angle θ is defined from the smaller particle.

4. Fully resolved model

The approach used in the present effort is quite different from percolation theory. The composite structure is synthesized by assembling a relatively small set of particles (hundreds of particles) into a cubical region (typically a few microns on a side). Neighboring particles may overlap to approximate sintering. The particle array is then discretized (here, a tetrahedral mesh as illustrated in Fig. 3) such that a diffusive transport equation that is resolved on the sub-particle scale can be solved. In this case, the intrinsic material properties are used (i.e., the conductivity σ_m^0, not an effective conductivity σ_m^{e}). This approach accounts directly for particle shapes and geometrical effects such as necking between particles. Because there is a certain randomness in assembling the particle arrays, many realizations are needed to deliver statistically valid results.

The process to determine the effective conductivity begins by solving a charge-conservation equation

$$\nabla \cdot (\sigma_m^0 \nabla \Phi_m) = 0 \tag{7}$$

within the particle network. Because the intent here is only to determine effective conductivities, the charge-transfer chemistry is neglected. Solution requires boundary conditions on all faces of the cube. For example, on the top face $\partial\Omega_{\mathrm{T}}$ the electrical potential Φ_m is imposed as $\Phi_m = 1$ and on the bottom face $\partial\Omega_{\mathrm{B}}$, $\Phi_m = 0$. The side walls are assumed to be symmetry boundaries, specified

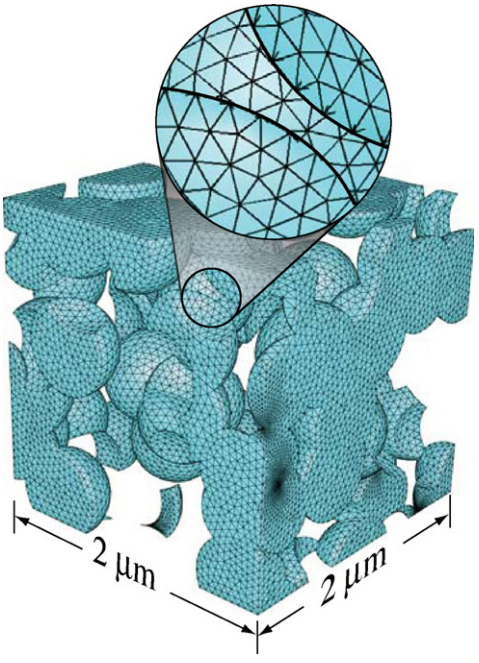

Fig. 3. A collection of randomly packed spheres with a tetrahedral mesh shown on the particle surfaces.

as $\mathbf{n} \cdot \nabla \Phi_m = 0$, where $\mathbf{n}$ is a unit vector normal to the face. With a solution in hand, the axial component of the current through the particle network can be evaluated at either the top or bottom surface as

$$J_m^e = \int_{\partial\Omega_T} \sigma_m^0 \mathbf{n} \cdot \nabla \Phi_m dA = \int_{\partial\Omega_B} \sigma_m^0 \mathbf{n} \cdot \nabla \Phi_m dA, \quad (8)$$

The integral considers only the particle-interface areas intersecting the top or bottom surfaces through which there can be conduction.

The effective conductivity is defined to be the ratio of the axial current through the particle network and the axial current through a solid cube of the parent material. Axial current through a solid cube is evaluated simply as

$$J_m^0 = A\sigma_m^0 \frac{d\Phi_m}{dx}, \quad (9)$$

where A is cross-sectional area of the dense cube. Thus, the effective conductivities are evaluated as

$$\sigma_m^e = \frac{J_m^e}{J_m^0}. \quad (10)$$

5. Particle-packing algorithms

Constructing particle-scale models depends upon an algorithm to synthesize a particle and pore structure. For composite electrodes, such a structure is composed of two particle types (i.e., ion-conducting and electron-conducting) and pore space. This is most often accomplished using various packed-sphere models [32,25], although at least one group uses rectangular elements [11]. Monodispersed spherical particles are used here, but the approach is fully capable of using different shapes and polydispersed sizes. In this paper two different approaches are developed for establishing the particle positions; one is based upon a discrete-element method and the other is a random packing.

Although random packing of simple shapes is convenient, it should be recognized that real structures may not be so simply represented. Actual electrode fabrication begins by ball milling powders (nominally spherical particles) together with binders. In the case of a Ni–YSZ anode, the Ni is in the form of nickel oxide, NiO. The resulting slurry is formed into a nominal shape (e.g., tube) by casting or extrusion. The part is then dried and fired at high temperature, which causes the particles to sinter together. In some cases the slurry may contain a pore former (e.g., graphite), which is burned out during firing. Pore formers are used to create pore spaces that are larger than would otherwise be present using the functional powders alone. In a Ni–YSZ structure, the NiO must be reduced to Ni before application in the fuel cell. The NiO reduction is accomplished by reaction with H_2 at high temperature. Because the NiO occupies a much larger volume than does the Ni, the reduction process also opens pore space. Given such a fabrication process, it is easy anticipate that the resulting structure may not be represented simply as an assembly of packed spheres.

Fig. 4 shows the comparison of a microscopic image of an SOFC with a model electrode structures based upon randomly packed spheres. It is evident that packed spheres, or any other simple shape, are not entirely adequate in representing the real structure. Nevertheless, models based upon packed spheres do provide valuable quantitative insight about how electrode performance depends upon microstructure. In addition to seeking physically representative packing, a further objective here is to pack particles in ways that are consistent with assumptions made in models based upon percolation theory. This provides a basis for comparing resolved-particle results with percolation-theory predictions.

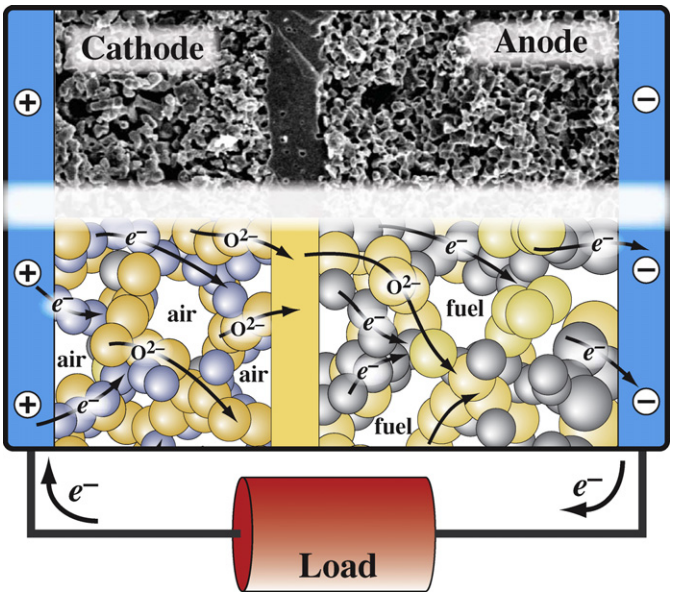

Fig. 4. Scanning electron microscope (SEM) image of an SOFC membrane-electrode assembly (top) and composite electrode representations based upon randomly packed spheres.

5.1. Discrete element method

The discrete element method (DEM) is a well-established method for predicting the evolution of particle trajectories, accounting for interparticle collisions and other relevant forces [33]. The method provides a general framework for solving a set of ordinary differential equations that express the Newtonian equations of motion for individual particles. Martin et al. [34] first used a DEM approach to represent SOFC anodes, focusing on particle deformation during sintering.

Briefly, as implemented here, the DEM packing algorithm involves the following steps:

- Define a tall vertical rectangular domain, typically a few microns on short sides. That is the height z is around three times greater than the x and y dimensions.
- At the top of the rectangular domain (x–y plane) introduce small (typically fraction of a micron) spherical particles with random initial positions and velocities. Each particle is identified as either an ion- or electron-conducting particle. The particles fall under the influences of gravity and interactions with other particles.
- Solve Lagrangian equations of motion to predict the particle trajectory until the particle comes to rest in the lower portion of the rectangular domain.
- As a particle moves its motion is affected by the net forces and torques it encounters by colliding with other particles and the domain walls.
- The filling process is terminated when the lower portion of the rectangular domain is filled with particles at rest, forming a nominal cubical domain.
- The DEM process alone produces a set of particles that touch, but do not overlap. To simulate sintering, the particle radii are expanded to achieve a certain level of overlap.

For the narrow purposes of producing particle packing, the particle contact forces are modeled using a relatively simple spring and dashpot analogy occurring over a finite time interval. A more detailed DEM simulation could incorporate a more physically realistic modeling of all contact interactions. However, because the objective of the present work is to use DEM simply as a means

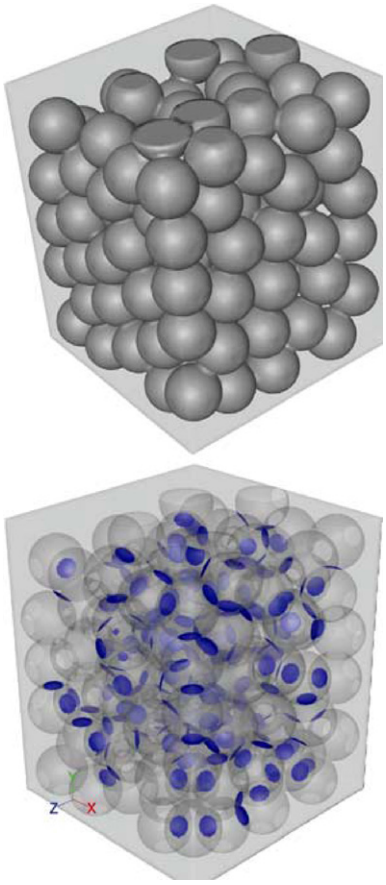

Fig. 5. Array of spheres produced from the DEM packing algorithm. The lower image highlights the contact areas between the spheres after artificial sintering.

to generate a packing configuration, there is no need to be concerned with potentially complex particle-interaction forces. The particle masses as well as the spring and dashpot parameters are set somewhat arbitrarily to achieve reasonable computation times.

The results reported in this paper use uniform particles with a radius of 0.3 μm. The bounding volume is chosen as 3.3 μm in the x and y directions. The filling process continues until the particles have filled the domain up to a z dimension about 3.3 μm. Once the particle positions are established the particle radii are increased to achieve a typical particle-intersection angle of 15° (Fig. 2). This procedure approximates a sintering process, and is consistent with approximations that are often made in percolation theory [31]. Fig. 5 shows a typical particle-packing configuration produced by the DEM method. The upper panel shows the particles packed inside the cubical domain. The lower panel highlights the contact area between particles.

Porosity, which is an important characteristic of the microstructure, is found by a sampling algorithm. A large sequence of randomly generated points (i.e., x, y, and z coordinates) within the cubical domain are generated. Each point is evaluated to determine if it is within a solid particle or not. With sufficient numbers of points, the porosity is established as the ratio of points that fall outside solid particles and the points that fall within solid particles. Points that fall within one particle diameter of the boundaries are discounted so as to reduce boundary effects. The average porosity is found to be about 32% for the DEM packing used here.

5.2. Random particle packing

The second approach for synthesizing a microstructure is based upon the random generation of particles within a cubical domain.

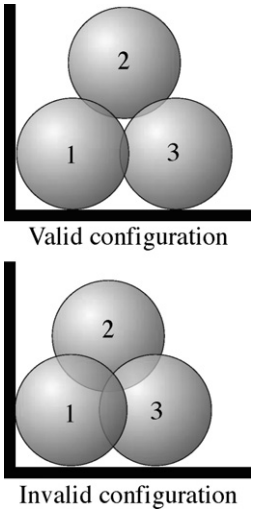

Fig. 6. Valid and invalid particle-packing configurations.

Similar approaches have been used previously for studying percolating clusters [28]. The algorithm begins by generating at random a trial position (i.e., x, y, and z coordinates) for a spherical particle within a cubical domain. The particle position is tested against a set of constraints to determine its validity. If valid, the particle is retained. Otherwise the trial particle is discarded. In either case, a new particle position is generated and tested for validity. The process continues until the cubical domain is filled with valid particles.

The packing constraints are stated as follows:

1. A valid particle must have contact or overlap with at least three neighboring particles and/or the domain boundaries.
2. The intersection perimeter between particles must be circular. In other words, as discussed below, a given particle cannot overlap simultaneously with more than one particle.
3. The intersection angles must be $0^\circ \leq \theta \leq 30^\circ$ (Fig. 2), with an average overlap angle of 15°.

Fig. 6 shows examples of valid and invalid particle intersections. In the upper panel sphere 1 satisfies constraints with respect to its contact with spheres 2 and 3 and surrounding domain boundaries. However, the configuration in the lower panel violates the second constraint because the intersection of spheres 1 and 2 is also intersected by sphere 3. The second constraint is imposed to generate configurations that are similar to the ones obtained from the DEM-based method and to be roughly consistent with common assumptions in percolation theory. However, this constraint is not necessary and could be relaxed to produce closer packing and smaller pore spaces.

Filling a cubical domain using the random-packing algorithm is a very lengthy process because most randomly generated positions fail to satisfy the packing criteria. However, the process is fully automated. To satisfy the first constraint, stable particles are initially positioned next to the bounding walls where three or more contact points are easily found within a nearly empty domain. As more and more particles are generated, the interior of the domain is successively filled. There is reason to expect from percolation theory that particle overlap angles (illustrated in Fig. 2) should be around 15° [27,35]. However, because the particles are generated randomly, a range of interaction angles between 0° and 30° is accepted, yielding an average overlap of about 15°.

The porosity of the resulting microstructure is calculated in exactly the same way as DEM. However due to the various

constraints the porosities are found to be about 47%, which is significantly higher than the porosities found via the DEM packing of around 32%. It should be recognized that it is possible to produce lower porosities (similar to those with the DEM-based method) by relaxing the above constraints. However, doing so would cause the particle-overlap characteristics in the resulting microstructure to be qualitatively different from the DEM-generated microstructure. Because it is interesting to compare the two packing methods, the random packing is constrained for the purposes of this paper. A porosity of 47% is relatively high for a typical SOFC electrode. However, the measurements reported by Iwai et al. [12] show porosities in this range.

5.3. Discretization

Once the particle positions are established, the next step is to discretize the structure. The particle coordinates and dimensions of the bounding domain are imported into the ANSYS GAMBIT mesh-generation software. Next, a set of spherical geometric solids representing electron-conducting and ion-conducting particles are generated along with the surrounding rectangular volume. A sequence of Boolean-intersection operations are performed on these primitives producing the final geometry comprising of overlapping particles and boundaries. An unstructured tetrahedral mesh is generated in the solid volumes. The complement of the solid volumes formed by the spheres represent the pore volumes. Although not used in the present paper, the pore regions can also be meshed for solving the fluid-transport equations. The three-phase boundaries can be automatically identified and the TPB lengths computed.

The unstructured tetrahedral meshing is entirely general and is in no way restricted to spherical particles or any other array of simple shapes. If a detailed geometric specification is available (e.g., from an experimental reconstruction), the electrode structure can be discretized. The simulation and analysis procedure is applied in just the same way as for the spherical-particle representations.

6. Results and discussion

The primary objective of this paper is to estimate effective conductivity. However, the model can also be used to evaluate the mean coordination number that is used in percolation theory (Eq. (4)). In percolation theory it is common to assume an average overall coordination number around $\bar{Z} = 6$. Both the coordination number and the percolation probability can be explicitly evaluated in the present fully resolved-particle model. Thus these two quantities can be used to provide further insight about percolation models and as partial validation of the resolved-particle model.

6.1. Coordination number

The coordination number is calculated directly once the particle positions are established. Because each instance of the particle-generation process produces a different geometric configuration, many such realizations are needed to obtain results that are statistically invariant with respect to the geometry and the particle sample size. It is expected that the results obtained from simulating a relatively small sample size for a large number of realizations should be virtually identical to that obtained from simulating a large sample size with fewer realizations. Two different sample sizes (150 and 300 particles) are simulated using the DEM-based model to investigate the influence of particle sample sizes on the coordination number. Neither of the packing algorithms described above is limited by the number of particles simulated. However, larger samples require greater computational resources for meshing and simulation, limiting the number of realizations that can be practically considered.

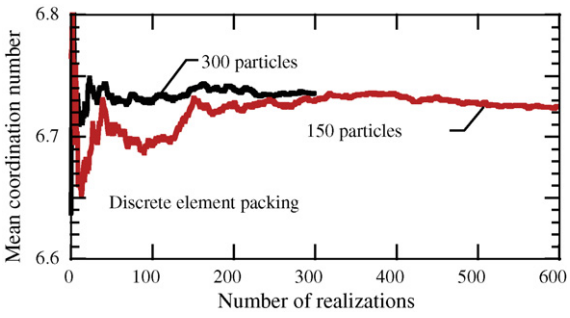

Fig. 7. Evolution of mean coordination number $\bar{Z}$ for 150 and 300 particles using the DEM packing.

The 150-particle samples are run for 600 realizations and the 300-particle samples are run for 300 different realizations resulting in the consideration of a total 90,000 particles for each sample size. A range of bins, initially empty and representing discrete coordination numbers, are set up at the beginning of the computations. Following a given instance of the particle-generation process, the coordination number for each particle is computed and the appropriate bin count is incremented. Next, the mean coordination number is computed for all particles and a running average is maintained over all realizations. The process is repeated until a quasi-steady value of the mean coordination number is achieved. This procedure effectively determines the number of realizations (and hence particle sample size) required to achieve a statistically invariant value of the mean coordination number. Additionally the probability distribution function (PDF) of the coordination number is obtained as a result of the simulations. Only particles which are situated at least one particle diameter away from the walls are considered in the coordination-number calculation, thus minimizing wall effects.

Fig. 7 shows the typical evolution of the mean coordination number as a function of the number of realizations for 150 and 300 particles with the DEM packing. The mean coordination number asymptotically approaches $\bar{Z} \approx 6.7$. This result confirms that the strategy of performing a large number of simulations with a limited sample size is theoretically sound. The final value of the coordination number is consistent with results reported by others [28].

Fig. 8 shows comparative histograms produced by the 150- and 300-particle simulations with the DEM packing. Once again it is evident that the PDF of coordination numbers obtained from the two sample sizes are virtually identical. Similar trends are also observed for the random-packing algorithm. Based upon experience with the DEM-packing and the random-packing algorithms, all subsequent simulations were performed with a sample size of 150 particles and 600 realizations.

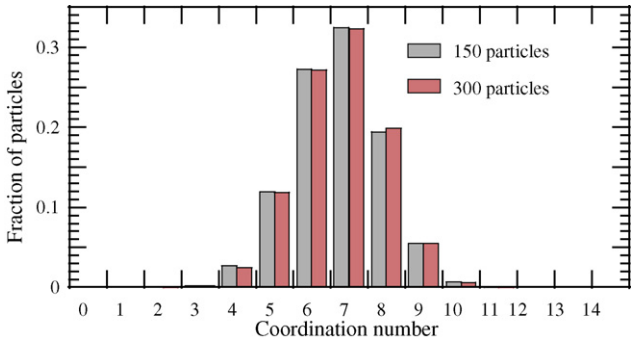

Fig. 8. Probability of mean coordination number $\bar{Z}$, comparing samples of 150 and 300 particles with DEM packing.

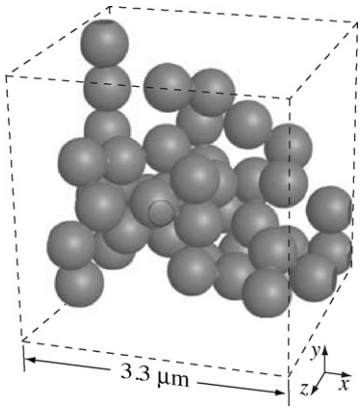

Fig. 9. A typical percolating cluster.

6.2. Percolation probability

Percolation probability plays an important role in evaluating effective three-phase-boundary length and effective conductivity. Once a set of particles have been generated, clusters can be identified, and the percolation probability evaluated. Comparing the directly evaluated percolation probabilities with percolation theory provides some partial validation of the resolved-particle algorithms.

An algorithm is formulated to identify distinct clusters of contiguous particles of a given type (i.e., ion-conducting or electron-conducting). List-based data structures are established to represent contiguous particles or clusters. Beginning with a particular particle, the algorithm keeps track of all particles that are connected directly or indirectly, thereby forming a contiguous cluster. The process is repeated for all particles. Finally all particles in the domain are assigned to unique clusters. Once individual clusters are identified, they are compared with the domain extents to isolate only those clusters that percolate throughout the domain in either the *x*-, *y*-, or *z*-direction. Fig. 9 shows a typical cluster spanning the domain in the *x*-direction, thus forming a continuous conduction pathway. The percolation probability for a given phase volume fraction is calculated as the fraction of cases when one or more percolating clusters are found.

Fig. 10 shows the percolation probabilities as functions of phase volume fraction. The resolved-particle models predict that the percolation probability increases more slowly as a function of phase volume fraction than the percolation theory (Eq. (4)). Moreover, the particle models predict higher percolation probability at low phase volume fraction. In other words, the percolation threshold occurs at lower phase volume fraction. Nevertheless, the resolved models predict the rapid increase in percolation probability in the volume-fraction range $0.3 < \psi_m < 0.5$, indicating that the computational approach provides a reasonable representation of the microstructure.

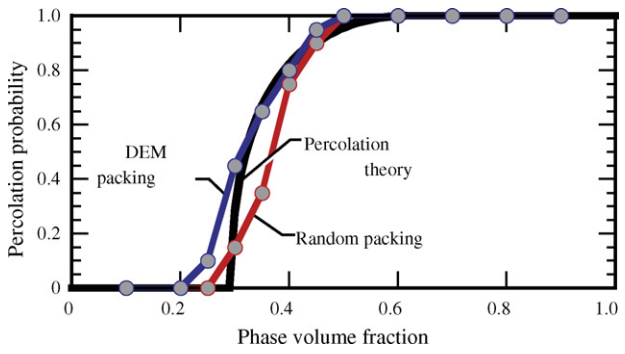

Fig. 10. Percolation probability as functions of solid-phase volume fraction, ψ_m.

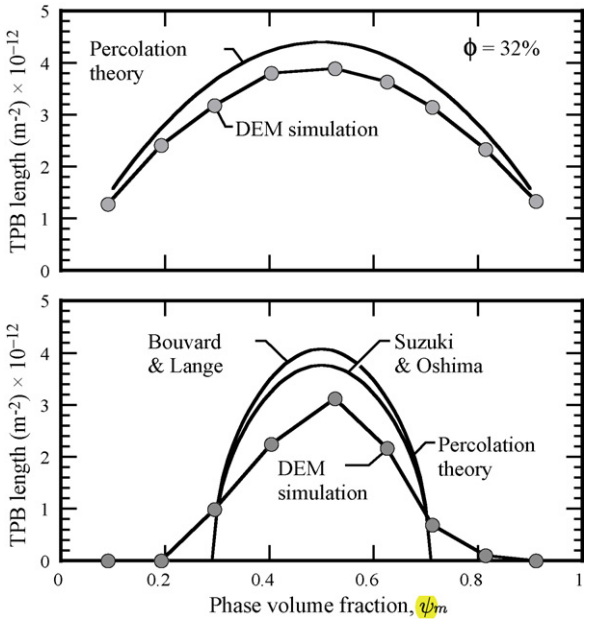

Fig. 11. Specific three-phase-boundary (TPB) lengths λ^{V}_{TPB} predicted by percolation theory (i.e., Eq. (5)) compared to the resolved-particle model with DEM packing. The percolated TPB lengths predicted by percolation theory use two alternatives (i.e., Eq. (3) or (4)) to evaluate the percolation probabilities.

6.3. Three-phase-boundary length

Accurate prediction of the three-phase-boundary (TPB) length is an important aspect of modeling charge-transfer chemistry in SOFCs. The TPB length is evaluated by discretizing the circles that are formed around the intersections between an ion-conducting and electron-conducting particles, and then counting the number of points on that boundary that are also shared by the adjoining pore volume.

Fig. 11 shows TPB lengths (i.e., length per unit volume) predicted by percolation theory and the DEM packing algorithm. For a three-phase boundary to be effective in charge transfer, both ions and electrons must be available. That is, there must be percolation for both the ion- and electron-conducting phases to the TPB. The upper panel in Fig. 11 is concerned with the entire TPB lengths, independent of whether there is percolation or not. The resolved model and the percolation theory (i.e., Eq. (5), assuming $P_{el} = P_{ed} = 1$) agree well, indicating that the geometric evaluation of complete TPB length is consistent with percolation theory. The lower panel of Fig. 11 is concerned with the percolated TPB length. Two percolation-theory results are shown, using Eqs. (3) (Bouvard and Lange [28]) and (4) (Suzuki and Oshima [30]) to evaluate the percolation probabilities. Owing to lack of percolation for one of the phases at high and low volume fractions, the percolated TPB shows a much narrower distribution than the complete TPB length. The DEM simulations agree reasonably well with the percolation theory, although the distribution functions are wider and the peak TPB length is somewhat lower.

Fig. 12 shows TPB lengths predicted by the random-packing algorithm. Because the porosity is higher than in the DEM simulations, the TPB lengths are generally smaller for the random packing. The widths of the percolated TPB distributions are comparable for the DEM and random-packing cases, but the predicted peak percolated TPB lengths are considerably lower than the percolation theory for the random-packing simulations.

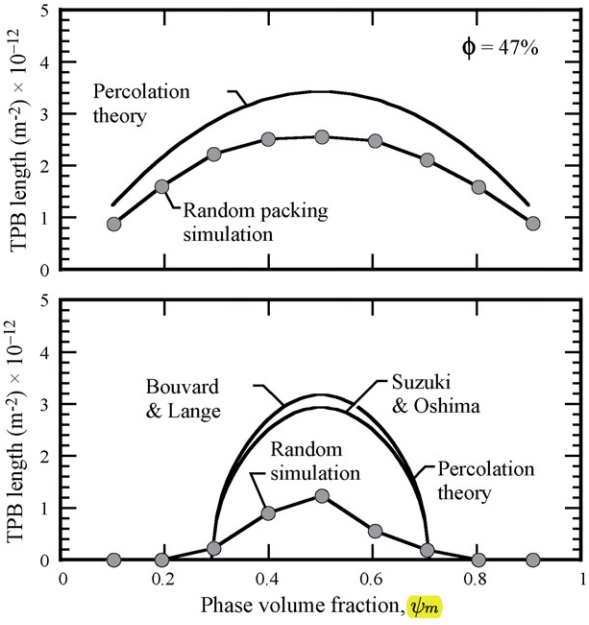

Fig. 12. Specific three-phase-boundary (TPB) lengths λ^{V}_{TPB} predicted by percolation theory (i.e., Eq. (5)) compared to the resolved-particle model with random packing. The percolated TPB lengths predicted by percolation theory use two alternatives (i.e., Eq. (3) or (4)) to evaluate the percolation probabilities.

6.4. Effective conductivity

The resolved-particle models evaluate the effective conductivity directly. However, based upon percolation theory, one can anticipate certain functional dependencies. Eq. (2) shows that the effective conductivity depends upon the percolation probability and the tortuosity of the conduction pathways (i.e., the Bruggeman factor, γ). The probability of a percolating cluster of a certain particle type increases with increasing particle volume fraction.

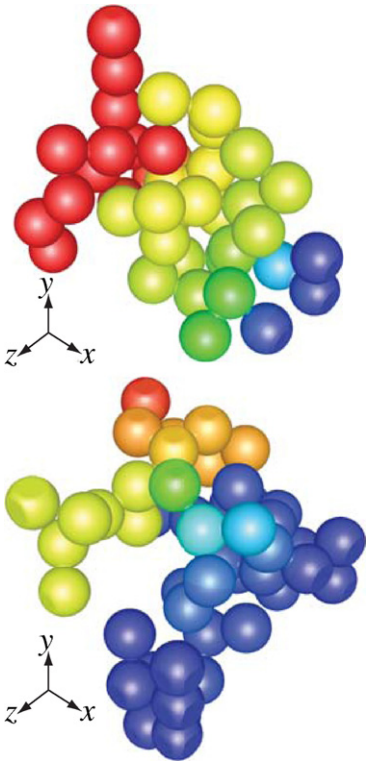

Fig. 13. Conduction in two different percolating clusters. Colors indicate electric potential, with red being high and blue being low. (For interpretation of the references to color in this figure legend, the reader is referred to the web version of the article.)

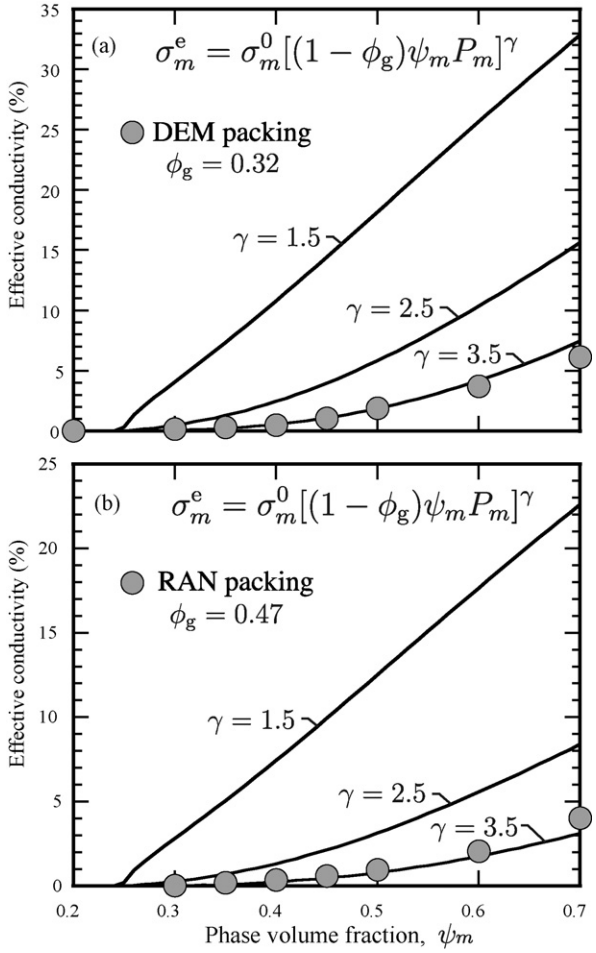

Fig. 14. Predicted effective conductivities σ^e_m as functions of solid-phase volume fraction.

The resolved-particle models are applied for a wide range of phase volume fractions. Once a percolating cluster is identified, a pure diffusion problem is solved for a generic scalar (e.g., electric potential) with Dirichlet boundary conditions specified at each end (Eq. (7)). Fig. 13 shows typical surface distributions of the scalar in clusters for two different realizations (particle configurations). To obtain statistically invariant results, the simulations are run for twenty distinct realizations corresponding to each phase volume fraction. The effective conductivity is defined as the ratio of the total current through the conducting clusters for a given phase volume fraction and the ideal current through the cubical volume (Eq. (10)).

Fig. 14 shows predicted effective conductivities as functions of phase volume fraction for both DEM and random packing. The DEM packing produces average porosity of $\phi_g = 0.32$ and the random packing produces average porosity of $\phi_g = 0.47$. The figure also shows comparisons with "standard" percolation theory (i.e., Eq. (2)), but using different values of the Bruggeman factor. It is evident that the commonly used value of $\gamma = 1.5$ produces much higher effective conductivities than those predicted by the fully resolved models. A value of $\gamma \approx 3.5$ is consistent with the resolved-particle simulations.

There is some evidence that the effective conductivity predicted by conventional percolation theory (i.e., Bruggeman exponent of

$\gamma = 1.5$) may be too high. Recent publications by Iwai et al. [12] and Wang et al. [36] are consistent with the present resolved-particle findings, showing significant deviations from percolation theory. Iwai et al. propose that the effective conductivity may be evaluated as [12]

$$\sigma_m^e = \sigma_m^0 \frac{(1-\phi_g)\psi_m}{\tau_m}, \quad (11)$$

where τ_m is a tortuosity factor. In this equation $(1-\phi_g)/\psi_m$ is the fraction of the entire volume occupied by phase m, whereas ψ_m is the volume fraction of the solid phases alone. Although the tortuosity factors reported by Iwai et al. are strongly anisotropic, even the least tortuous paths produce effective conductivities that are much lower than those predicted by Eq. (2).

Wang et al. [36] formulated stochastic representations of PEMFC composite cathodes, assuming the microstructure to be represented by randomly generated cubes. They simulated transport and charge transfer using a fully resolved model similar to the one developed in the present paper. Comparing the fully resolved results to a one-dimensional macromodel suggested a Bruggeman factor between 3.5 and 4.5. Thus, the Wang et al. results are also consistent with the present models.

The Bruggeman factor γ is intended to account for two separate phenomena. One is the convoluted nature of conduction pathways and second is the possibility of isolated non-percolating clusters that do not contribute to conduction. Although the percolation probability (i.e., the probability that at least one cluster will percolate) is unity for $\psi_m > 0.5$, there may be islands of non-percolating particles that are not taken into account by Eq. (2). The fully resolved models capture such islands and thus predict significantly lower values of effective conductivity than the percolation theory.

7. Conclusions

A fully resolved-particle-based model of composite electrodes has been developed and applied to predict average coordination numbers, percolation probabilities, TPB lengths, and effective conductivities of the packed-particle networks. Two different packing algorithms are used to synthesize microstructures from spherical particles, with both algorithms producing similar results. Once a particle-based microstructure is generated, the entire particle matrix is discretized with a tetrahedral mesh network. A charge-conservation equation is solved to predict current through the particle network. These results are then used derive an effective conductivity that is represented as a fraction of the intrinsic material conductivity and microstructural characteristics of the particle network.

The particle-packing algorithms are random, causing each realization of a particle packing to be different. Thus, multiple simulations are needed to develop statistically valid results. The results show that a few hundred particles with a few hundred realizations are sufficient to reduce statistical variations to within acceptable levels.

Coordination numbers, percolation probabilities, and TPB lengths can be evaluated based upon packing geometry alone. These results are found to be consistent with percolation theory, serving as partial validation of the model. The effective conductivities that are derived from the fully resolved simulations are especially valuable in larger scale models where the particle scale cannot be resolved. The effective conductivities are found to be significantly smaller than those predicted by standard percolation theory. However, using a Bruggeman factor of $\gamma = 3.5$ instead of the commonly used $\gamma = 1.5$ brings the percolation prediction in line with the fully resolved results.

The results in the present paper are concerned with uniform-diameter spherical particles. One reason for this choice is to compare results with percolation theory. However, the resolved-particle modeling approach accommodates different particle shapes and sizes, thus providing the capability to explore and evaluate innovative electrode architectures. Moreover, the model can be extended easily to evaluate fluid-phase transport through the pore volumes.

Acknowledgments

This effort was supported by the Office of Naval Research via an RTC grant (N00014-05-1-03339). The authors gratefully acknowledge Vaughan Thomas (California Institute of Technology) for insightful discussions about cluster-detection algorithms and Naresh Patre (ANSYS India) for automating the simulation procedure.

References

[1] F. Zhao, A.V. Virkar, J. Power Sources 141 (2005) 79–95.
[2] H. Zhu, R.J. Kee, J. Electrochem. Soc. 155 (7) (2008) B715–B729.
[3] H. Zhu, R.J. Kee, V.M. Janardhanan, O. Deutschmann, D.G. Goodwin, J. Electrochem. Soc. 152 (2005) A2427–A2440.
[4] J.R. Wilson, W. Kobsiriphat, R. Mendoza, H.Y. Chen, J.M. Hiller, D.J. Miller, K. Thornton, P.W. Voorhees, S.B. Adler, S.A. Barnett, Nat. Mater. 5 (2006) 541–544.
[5] D. Gostovic, J.R. Smith, D.P. Kundinger, K.S. Jones, E.D. Wachsman, Electrochem. Solid-State Lett. 10 (2007) B214–B217.
[6] J.R. Wilson, A.T. Duong, M. Gameiro, H. Chen, K. Thornton, D.R. Mumm, S.A. Barnett, Electrochem. Commun. 11 (2009) 1052–1056.
[7] J.R. Wilson, J.S. Cronin, A.T. Duong, S. Rukes, H. Chen, K. Thornton, D.R. Mumm, S.A. Barnett, J. Power Sources 195 (2010) 1829–1840.
[8] J.R. Wilson, M. Gameiro, K. Mischaikow, W. Kalies, P.W. Voorhees, S.A. Barnett, Microsc. Microanal. 15 (2009) 71–77.
[9] P.R. Shearing, J. Golbert, R.J. Chater, N.P. Brandon, Chem. Eng. Sci. 64 (2009) 2933–3928.
[10] J.R. Smith, A. Chen, D. Gostovic, D. Hickey, D. Kundinger, K.L. Duncan, R.T. DeHoff, K.S. Jones, E.D. Wachsman, Solid State Ionics 180 (2009) 90–98.
[11] B. Rüger, J. Joos, A. Weber, T. Carraro, E. Ivers-Tiffée, ECS Trans. 25 (2009) 1211–1220.
[12] H. Iwai, N. Shikazono, T. Matsui, H. Teshima, M. Kishimoto, R. Kishida, D. Hayashi, K. Matsuzaki, D. Kanno, M. Saito, H. Muroyama, K. Eguchi, N. Kasagi, H. Yoshida, J. Power Sources 195 (2010) 955–961.
[13] J.R. Izzo, A.S. Joshi, K.N. Grew, W.K.S. Chiu, A. Tkachuk, S.H. Wang, W. Yun Jr., J. Electrochem. Soc. 155 (2008) B504–B508.
[14] K. Grew, A.A. Peracchio, J.R. Izzo, W. Chiu, ECS Trans. 25 (2009) 1861–1870.
[15] S. Sunde, J. Electrochem. Soc. 143 (1996) 1930–1939.
[16] S. Sunde, J. Electrochem. Soc. 143 (1996) 1123–1132.
[17] L.C.R. Schneider, C.L. Martin, Y. Bultel, D. Bouvard, E. Siebert, Electrochim. Acta 52 (2006) 314–324.
[18] L.C.R. Schneider, C.L. Martin, Y. Bultel, L. Dessemond, D. Bouvard, Electrochim. Acta 52 (2007) 3190–3198.
[19] A.S. Martinez, J. Brouwer, Electrochim. Acta 53 (2008) 3597–3609.
[20] Y. Suzue, N. Shikazono, N. Kasagi, J. Power Sources 184 (2008) 52–59.
[21] A. Lanzini, P. Leone, P. Asinari, J. Power Sources 194 (2009) 408–422.
[22] U. Doraswami, P. Shearing, N. Droushiotis, K. Li, N.P. Brandon, G.H. Kelsall, Solid State Ionics, in press, doi:10.1016/j.ssi.2009.10.013.
[23] P. Asinari, M.C. Quaglia, M.R. von Sparkovsky, B.V. Kasula, J. Power Sources 170 (2007) 359–375.
[24] A.S. Joshi, K.N. Grew, A.A. Peracchio, W.K.S. Chiu, J. Power Sources 164 (2007) 631–638.
[25] J. Golbert, C.A. Adjiman, N.P. Brandon, Ind. Eng. Chem. Res. 47 (2008) 7693–7699.
[26] B. Kenney, M. Valdmanis, C. Baker, J.G. Pharoah, K. Karan, J. Power Sources 189 (2009) 1051–1059.
[27] D.H. Jeon, J.H. Nam, C.J. Kim, J. Electrochem. Soc. 153 (2) (2006) A406–A417.
[28] D. Bouvard, F.F. Lange, Acta Metall. Mater. 39 (1991) 3083–3090.
[29] C.H. Kuo, P.K. Gupta, Acta Metall. Mater. 43 (1995) 397–403.
[30] M. Suzuki, T. Oshima, Powder Technol. 35 (1983) 159–166.
[31] D. Chen, Z. Lin, H. Zhu, R.J. Kee, J. Power Sources 191 (2009) 240–252.
[32] C. Metcalfe, O. Kesler, T. Rivard, F. Gitzhofer, N. Abatzoglou, ECS Trans. 25 (2009) 1185–1194.
[33] P.A. Cundall, A. Strack, Geotechnique 29 (1979) 47–65.
[34] C.L. Martin, D. Bouvard, S. Shima, J. Mech. Phys. Solids 51 (2003) 667–693.
[35] P. Costamagna, P. Costa, V. Antonucci, Electrochim. Acta 43 (1998) 375–394.
[36] G. Wang, P.P. Mukherjee, C.-Y. Wang, Electrochim. Acta 51 (2006) 3151–3160.